Effect of Network Relaxation on Void Propagation and Failure in Isotactic Polypropylene at Large Strain

Bing Na, Ruihua Lv, Wenfei Xu

Department of Materials Science and Engineering, East China Institute of Technology, Fuzhou 344000, People's Republic of China

Received 9 September 2008; accepted 3 April 2009
DOI 10.1002/app.30532
Published online 27 May 2009 in Wiley InterScience (www.interscience.wiley.com).

ABSTRACT: The important role of network relaxation in the voiding and fracture toughness of isotactic polypropylene (iPP) has been explored with video-aid tensile tests, two-dimensional small-angle X-ray scattering (2D-SAXS) measurements, and morphological observations. The results indicated that macroscopic volume dilatation related to voiding became lower during large deformation of iPP sample with rich γ phase (denoted as γ-iPP) cooled at 1°C/min, compared with one with exclusive α form (referred to α-iPP) quenched in air. Furthermore, void propagation perpendicular to the tensile direction, demonstrated by Guinier approximation analysis of 2D-SAXS results, was suppressed to a large extent in such a γ-iPP sample. Less network relaxation, resulted from its peculiar crystalline and amorphous phases, was responsible for lower volume dilatation and slower void propagation in the γ-iPP sample. Meanwhile, less network relaxation and suppressed transverse void propagation contributed to higher toughness in the γ-iPP sample. © 2009 Wiley Periodicals, Inc. J Appl Polym Sci 113: 4092–4099, 2009

Key words: network relaxation; void propagation; γ-iPP

INTRODUCTION

The key issue in understanding the relationship between microstructure and deformation behaviors in isotactic polypropylene (iPP) arises from the presence of a two-phased structure with crystalline and amorphous domains arranged alternatively.[1–3] With numerous efforts, the structural evolution and deformation mechanisms have been elucidated to a large extent. The deformation is first accommodated in the interlamellar amorphous phase, followed by the intensive chain slip in crystals on yielding. Finally, lamellar fragmentation and fibrillation set in at large strain. Simultaneously, molecular chains in the amorphous phase are gradually stretched.[4] Despite the complicate structural evolution in individual crystalline and amorphous phase, in a global view, the deformation of isotactic polypropylene at large strain can be viewed as the stretching of a network set up by the trapped chain entanglements in the amorphous layer and by the physical cross-links from crystallites. This viewpoint gives deep insight into the deformation behaviors in isotactic polypropylene and can find its origin in the rubber elasticity theory at moderate strain.[5] In addition, such a network may be destroyed beyond a certain strain through disentanglement in the amorphous phase or chain pullout from the adhered crystals.

Significant stress whitening is usually observed in the tensile deformation and fracture tests of isotactic polypropylene because of the presence of normal stress under tension.[6–8] It originates from noncohesive damage mechanisms, namely cavitation, at microscopic scale, which has been demonstrated by volume dilatation, small-angle X-ray scattering (SAXS) and morphological observations. Cavitation sets in around yield point and depends on the yield stress of crystals.[6] Voids can be readily nucleated via longitudinal separation between adjacent lamellae with normal parallel to the tensile direction (equatorial region) or disruption of blocky substructure of the crystalline lamellae with normal perpendicular to the stretching direction (polar region).[9] Once nucleated, the nascent voids can be enlarged under straining and finally becomes elongated along tensile direction. However, the deep understanding of void propagation at large strain has not been achieved yet. The relationship between void propagation and structural evolution is still absent, though void nucleation on yielding is solely triggered by the crystalline phase (including lamellar thickness, lamellar orientation, and crystallinity).

Correspondence to: B. Na (bingnash@163.com).

Contract grant sponsor: National Natural Science Foundation of China; contract grant number: 20704006.
Contract grant sponsor: Natural Science Foundation of Jiangxi, China; contract grant number: 0650009.
Contract grant sponsor: The Project of Jiangxi Provincial Department of Education; contract grant number: GJJ08295.
This research is also subsidized by the Opening Project of the State Key Laboratory of Polymer Materials Engineering (Sichuan University).

At atmospheric conditions, isotactic polypropylene with chain errors (i.e., co-unit, stereoirregularity, etc.) can crystallize into the γ phase from melt, which is favored by high crystallization temperature or slow cooling rate due to kinetic limitation.[10–12] Unlike α form, the chain packing in the orthorhombic unit cell of γ phase is nonparallel. Instead, the direction of the chain axis in adjacent bilayers is tilted by approximately 80° against each other and approximately 40° with respect to the lamellar normal. The special chain packing in the unit cell, in turn, suppresses the chain folding back into the same lamellae and, thus, increases the fraction of tie chains between adjacent lamellae.[13] The peculiar texture in the γ-iPP sample is responsible for its superior mechanical properties, as demonstrated in a recent study by Lezak et al.[14] on the plane strain compression of γ-iPP crystallized from homopolymer at high pressure.

In this study, iPP samples with rich γ phase or α-form have been prepared from the same copolymer by adopting different cooling rate. The main purpose is to understand the relationship between microstructure and mechanical behaviors in isotactic polypropylene. Our results indicate that void propagation at large strain is suppressed in the iPP sample with rich γ phase as a result of less network relaxation, which, in turn, is responsible for its superior fracture toughness.

EXPERIMENTAL SECTION

Materials and sample preparation

A commercial Ziegler-Natta catalyzed isotactic polypropylene copolymer with 3.7 wt % ethylene co-unit, supplied by Beijing Chemical Institute China, was used in the study. It had a weight-average molecular weight (M_w) of 801 kg/mol, a M_w/M_n of 5.0 and a melt flow index of 0.16 g/10 min (230°C/2.16 kg). Plaques with a thickness of 0.5 and 4 mm, respectively, were compression molded from pellets in a hot press with a temperature of 200°C and a pressure of 2 MPa. As stated in the introduction section, the formation of γ phase in iPP copolymer was favored by high crystallization temperature or slow cooling rate, whereas low crystallization temperature or rapid cooling promotes the formation of α-form in the same copolymer. Therefore, the molten plaques were cooled at 1°C/min and quenched in air to obtain samples with rich γ phase and exclusive α-form, respectively, after being held for 5 min in the press. Note that 4-m thick plaques were only used for notched Izod impact tests.

Structural characterization

XRD

X-ray diffraction was measured on an X-ray diffractometer equipped with an X-ray generator and a goniometer. The X-rays were generated at 35 kV and 60 mA and the wavelength of the monochromated X-ray from Cu K_α radiation was 0.154 nm.

DSC

The melting behaviors of both γ-iPP and α-iPP samples were registered at a heating rate of 10°C/min in a nitrogen atmosphere using a NETZSCH DSC 204, indium calibrated.

2D-SAXS

Two-dimensional SAXS measurements were performed using an in-house setup with a rotating anode X-ray generator equipped with two parabolic multilayer mirrors, giving a highly parallel beam of monochromatic Cu Kα radiation ($\lambda = 0.154$ nm). The SAXS intensity was collected with a two-dimensional gas-filled wire detector. The distance of sample to the detector was 1.38 m.

TOM

The damage zone region ahead of notches in the double edge–notched tension (DENT) samples was examined by a transmission optical microscopy under bright field. Before observation, the DENT samples were polished to about 50 μ in thickness.

SEM

The fracture surface of samples subjected to Izod impact tests was observed by a JEOL scanning electron microscopy. All specimens were coated with gold before SEM observation.

Free shrinkage

The tensile-deformed samples with ink marks were placed between two glass slides that were held together with paper clips at their edges and subsequently were placed in an oven with a temperature of 180°C for 10 min to achieve total shrinkage. To prevent molten samples from adhering to the glass plates, fine talc powder was used to cover the internal surfaces of the glass plates. Thereafter, the sample length between two adjacent ink marks preprinted on the samples was measured using a CCD camera. The permanent strain ε_p, defined as the natural logarithm of the ratio of remained length to the initial one, was adopted to characterize the network relaxation.

Mechanical tests

Video-aid tensile tests

Uniaxial tensile tests were performed on the dog-bone samples (4 mm width × 6 mm gage length)

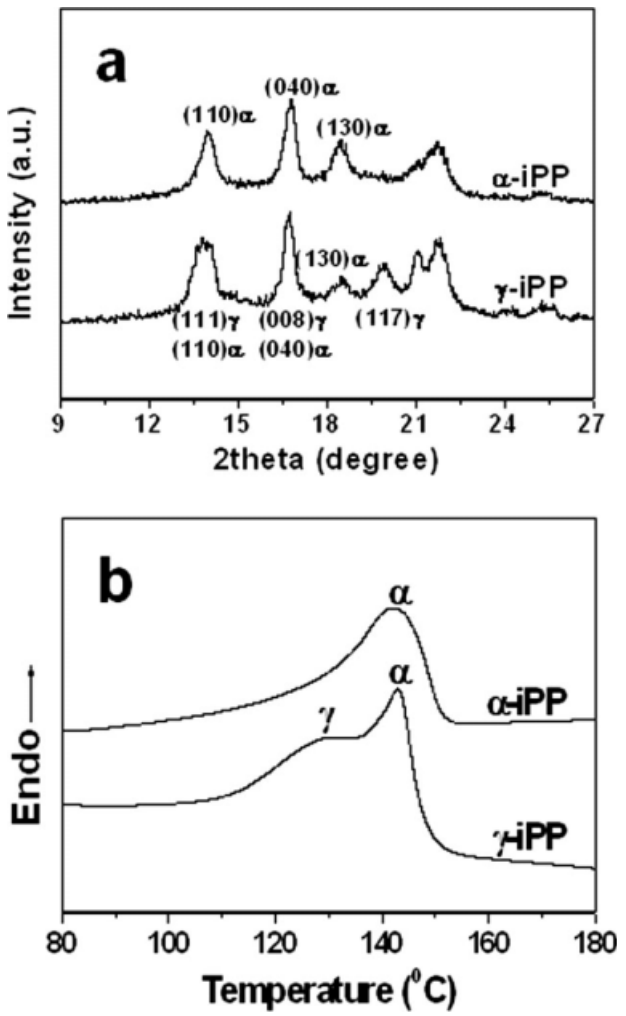

Figure 1 XRD profiles (a) and melting traces (b) recorded from γ-iPP and α-iPP sample, respectively.

using a universal testing machine at room temperature with a crosshead speed of 2 mm/min. To obtain true stress and true strain, a CCD camera (1280 pixel ×1024 pixel), equipped with a tunable magnification lens, was adopted to monitor the space change of desired ink marks preprinted on the samples during stretching. The initial distance of two adjacent ink marks was 0.5 mm. With knowledge of transient length and width of the sample, true stress, Hencky strain and Hencky volume strain could be simultaneously obtained. Note that transverse isotropy was assumed in the data treatment. Detail descriptions could be found in our previous study.[15]

EWF

Essential work of fracture (EWF) test was conducted by uniaxial tensile deformation of the deeply double edge–notched (DENT) samples at a crosshead of 2 mm/min. For meeting the demands of plane stress and free constraint of boundary, the ligament lengths of DENT specimens were varied between 3 and 11 mm. The detail experimental procedure could be found elsewhere.[15,16]

Notched Izod impact tests

The strips with a width of 10 mm were first machined from the 4-mm thick plates and then standard notches were introduced. The loading speed of impact tester was 3.5 m/s.

RESULTS AND DISCUSSION

Initial structure

Figure 1 is the X-ray diffraction (XRD) and differential scanning calorimetry (DSC) results for samples cooled at 1°C/min and quenched in air from melt, respectively. The attribution of most reflections in the XRD profiles and endothermic peaks in the DSC profiles is indicated in each legend. As expected, the formation of γ phase or α-form on cooling in the same iPP copolymer depends on the crystallization

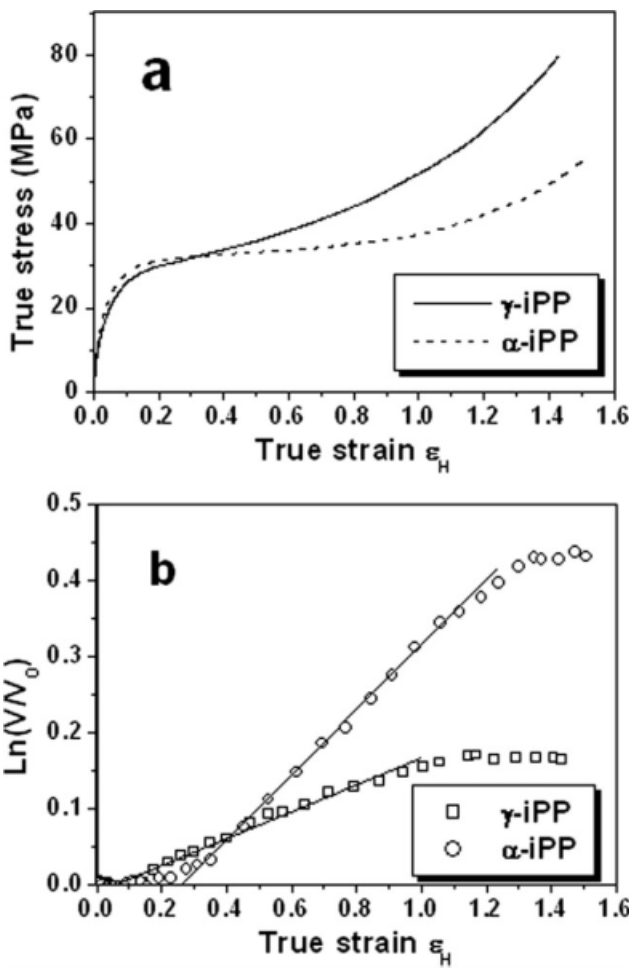

Figure 2 True stress strain dependence (a) and volume strain (b) obtained from tensile deformation of γ-iPP and α- iPP sample, respectively.

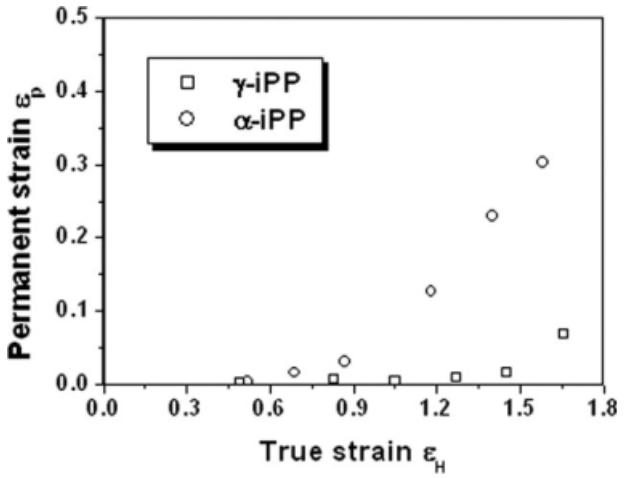

Figure 3 Permanent strains remaining in the γ-iPP (square) and α-iPP (circle) sample, respectively, after being held at 180°C for 10 min.

conditions. Abundant γ phase, with a characteristic reflection (117) at $2\theta = 20.1°$, is formed in the sample cooled at 1°C/min (denoted as γ-iPP), whereas only α form is observed in the sample quenched in air (referred to α-iPP). The XRD results further confirm that the formation of γ phase is favored by the slow cooling rate where the chain folding, which lead to formation of α-form is largely prevented, which has been well documented in the literatures.[10–13] Similarly, the formation of γ phase in the γ-iPP sample is also evidenced by the DSC results. The γ phase presents itself as a lower endothermic peak in the melting trace due to its lower thermal stability,[17] compared with the α counterpart. In addition, from the XRD profiles, the crystallinity is also deduced, which is 0.39 and 0.30 for γ-iPP and α-iPP sample, respectively. The higher crystallinity in the γ-iPP sample should be related to the slow cooling rate during sample preparation.

Tensile behaviors

Figure 2 is true stress strain dependence and volume strain during tensile deformation of γ-iPP and α- iPP sample, respectively. Different mechanical responses are observed in the above-referred samples. Despite the similar strain softening and yield behaviors, more significant strain hardening at large strain is presented in the γ-iPP sample. Three factors should be responsible for it. First, higher strain hardening in the γ-iPP sample in nature originates from its higher fraction of tie chains interconnecting adjacent lamellae[13] as well as from its higher amount of crystallites acting as physical cross-links according to the rubber elasticity theory.[5] Second, under stretching, the initial entangled network can be destroyed to some extent mostly due to chain pullout from the adhered crystals, and, thus, strain hardening is weakened. Once network relaxation occurs, the deformed sample cannot recover to its original length even if being heated up to the melting point.[18,19] To clarify it, thermal shrinkage at 180°C is conducted for both γ-iPP and α- iPP samples deformed to various strains and the corresponding permanent strain is collected in Figure 3. As expected, less network relaxation occurs in the γ-iPP sample with higher fraction of tie chain interconnecting adjacent lamellae. The clumsy chain errors included in the lamellae can further preclude the chain pullout from crystallites to large extent as a result of steric hindrance.[20] Third, significant volume dilatation can reduce the stress accumulation and the strain hardening due to microporosity, and, thus, suppressed volume dilatation at large strain is another factor for higher strain hardening in the γ-iPP sample.

As demonstrated in the tensile deformation of high-density polyethylene[21,22] and isotactic polypropylene with α-form,[9] volume dilatation during

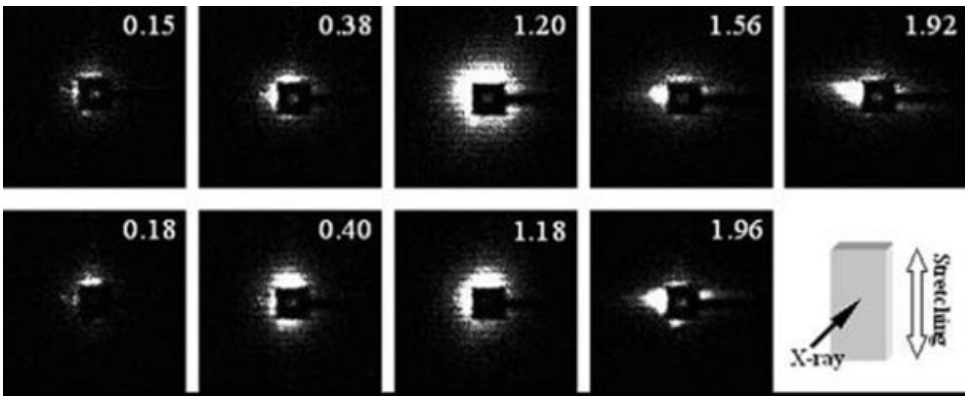

Figure 4 2D-SAXS patterns from γ-iPP (top) and α-iPP (bottom) sample, respectively, deformed to various true strains (indicated by the number in each legend). The incident beam is along the sample thickness. Note that the scattering of the undeformed states has been subtracted from the scattering of deformed samples as a background.

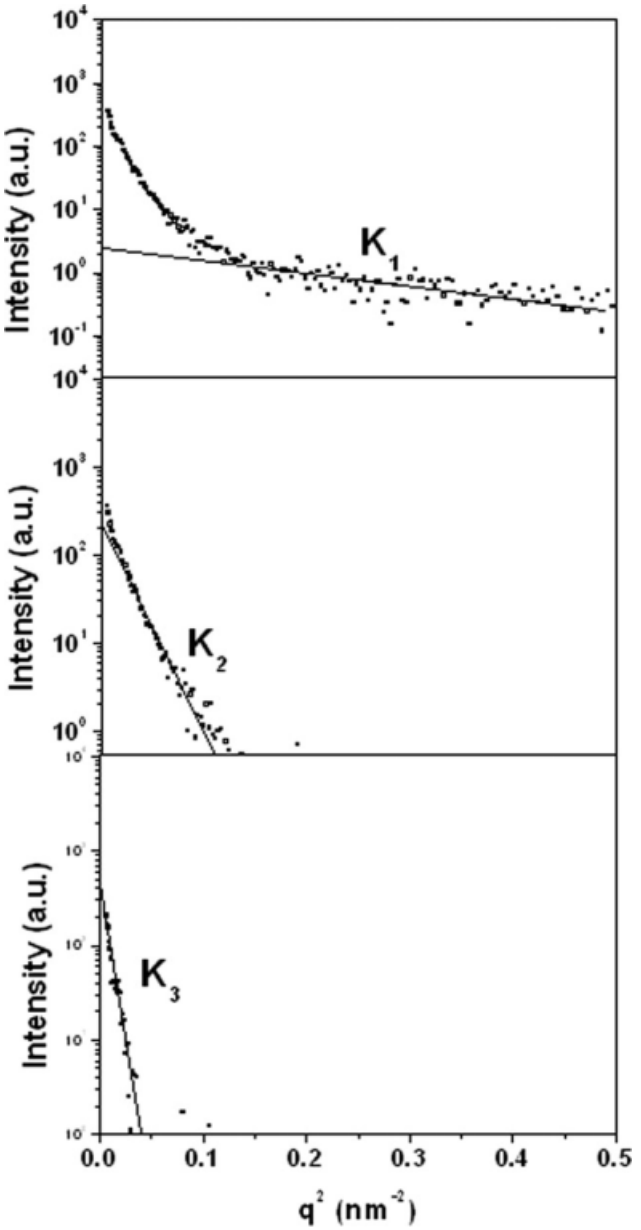

Figure 5 Typical Guinier plots for γ-iPP sample along the equatorial direction at a true strain of 1.20. Note that K_1, K_2, and K_3 correspond to three void groups with different size.

stretching mostly arises from cavitation in the amorphous phase at microscale because of the presence of negative pressure. Cavitation sets in around yield point and becomes apparent with increasing crystallinity, which is the fact observed for the γ-iPP sample. Once nucleated, voids can propagate parallel and perpendicular to the tensile direction simultaneously with further straining, which cannot be described by the overall volume strain shown in Figure 2(b). In the following section, therefore, attentions are paid to the void propagation especially perpendicular to the tensile direction at microscale with the aid of 2D-SAXS measurements in detail.

Figure 4 is the 2D-SAXS patterns obtained from the γ-iPP and α-iPP sample deformed to various true strains, respectively. Note that the scattering of the undeformed states has been subtracted from the scattering of deformed samples as a background. Consistent with the volume dilatation shown in Figure 2(b), intensive scattering, resulted from high electron density difference between void and polymeric matrix,[23] is observed in all deformed samples at low scattering vector q, defined as $q = 4\pi \sin \theta/\lambda$ (where θ is the scattering angle and λ is the wavelength of X-ray). Scattering from voids appears in both meridional and equatorial direction and finally concentrates in the equatorial direction, irrespective of the γ-iPP or α-iPP sample. It is indicated that newly formed voids are first enlarged parallel and perpendicular to the tensile direction simultaneously and then become elongated along the tensile direction. The large size of elongated voids along the tensile direction with strain beyond about 1.2 is mostly out of the detecting range of 2D-SAXS (which is about 80 nm in our case) and thus has little contribution to the scattering along the tensile direction. Therefore, only the scattering profiles perpendicular to the tensile direction are further analyzed by Guinier approximation to obtain the information about transverse void propagation with strain.[9,23]

$$I = \sum_{i=1}^{n} K_i \exp(-R_i^2 q^2/3) \tag{1}$$

$$N_i = AK_i/R_i^3 \tag{2}$$

$$f_i = N_i / \sum_{1}^{n} N_i \tag{3}$$

where K_i is proportional to the volume of voids in the ith group, R_i is the radius of gyration, A is a constant depending on the geometry of inclusions, N_i is the number of voids, and f_i is the fraction of voids in the ith group. A plot of ln I versus q^2 can yield two parameters: R_i from the slop and K_i from the intersection at $q^2 = 0$. Figure 5 is such a plot obtained from λ-iPP sample at a strain of 1.2 along equatorial direction. It is apparent that the relation of ln I versus q^2 is not linear in a global sense. It means that the size of voids in the deformed samples is not uniform and has a continuous distribution. In this case, for simplicity, the voids are divided into three groups located in various q ranges: K_1, K_2, and K_3, as shown in Figure 5. Note that the typical size of voids, defined as $2R_i$, is about 6, 24, and 50 nm for K_1, K_2, and K_3 group, respectively. Detailed procedure of data analysis is presented in the previous studies of Ijichi et al[23] and Yamashita.[24] The absolute amount of void in each group cannot be determined

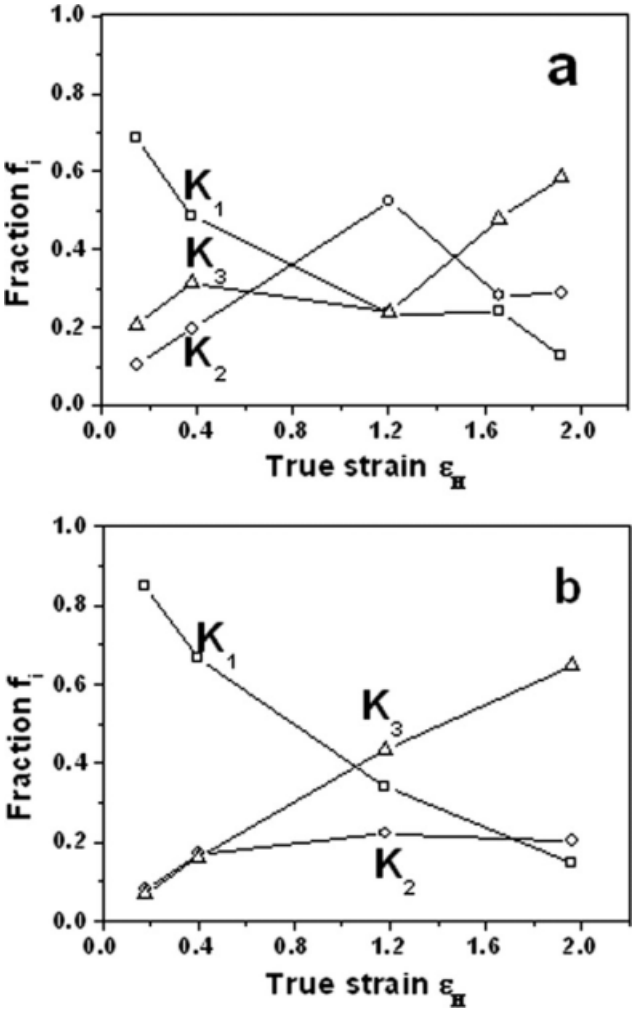

Figure 6 Relative fraction of voids with indicated size group (K_1, K_2, and K_3) in the γ-iPP (a) and α-iPP (b) sample perpendicular to the tensile direction.

because several parameters in eqs. (1)–(3) remain unknown and thus only the relative fraction of voids is considered (Fig. 6). As expected, the fraction of voids with smallest size (group K_1) decreases monotonically with strain in both γ-iPP and α-iPP samples, indicating that the newly formed voids are gradually enlarged in the equatorial direction (also evidenced by the increased fraction of voids with large size in the group K_2 and K_3). The most significant difference of transverse void propagation between γ-iPP and α-iPP sample is the evolution of voids with largest size (group K_3) with strain no more than about 1.2. More rapid void propagation perpendicular to the tensile direction is observed in the α-iPP sample, whereas void propagation in the γ-iPP sample is arrested to large extent (manifested by higher fraction of voids with moderate size in group K_2). The void propagation with strain detected by the 2D-SAXS measurements is consistent with the volume strain shown in Figure 2(b), although the sensitivity and detectable size of voids are different for both above-mentioned methods. As stated in a study on the tensile deformation of oriented high-density polyethylene, void propagation perpendicular to the tensile direction depends on the constraints in the

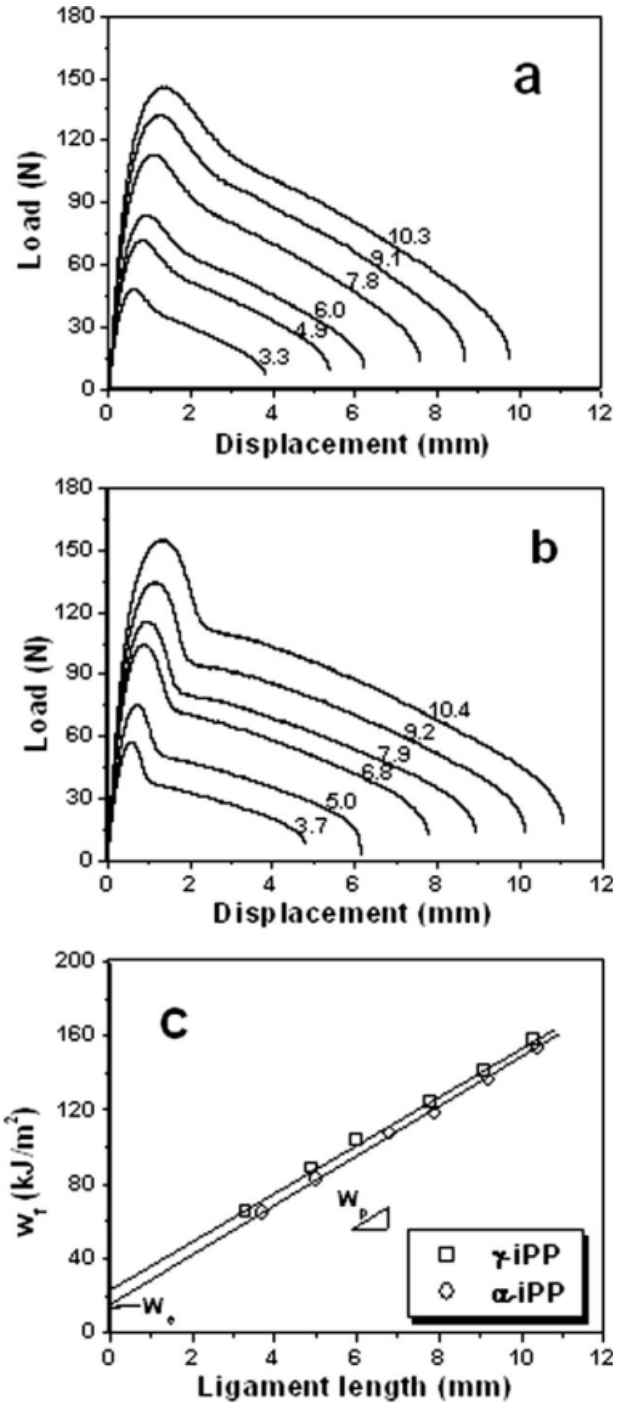

Figure 7 The load-displacement profiles registered from γ-iPP (a) and α-iPP (b) samples with different ligament length (indicated by the number on each curve). The dependence of w_f as a function of ligament length is presented in subpart (c). A value of w_e can be deduced from the interception at zero ligament length.

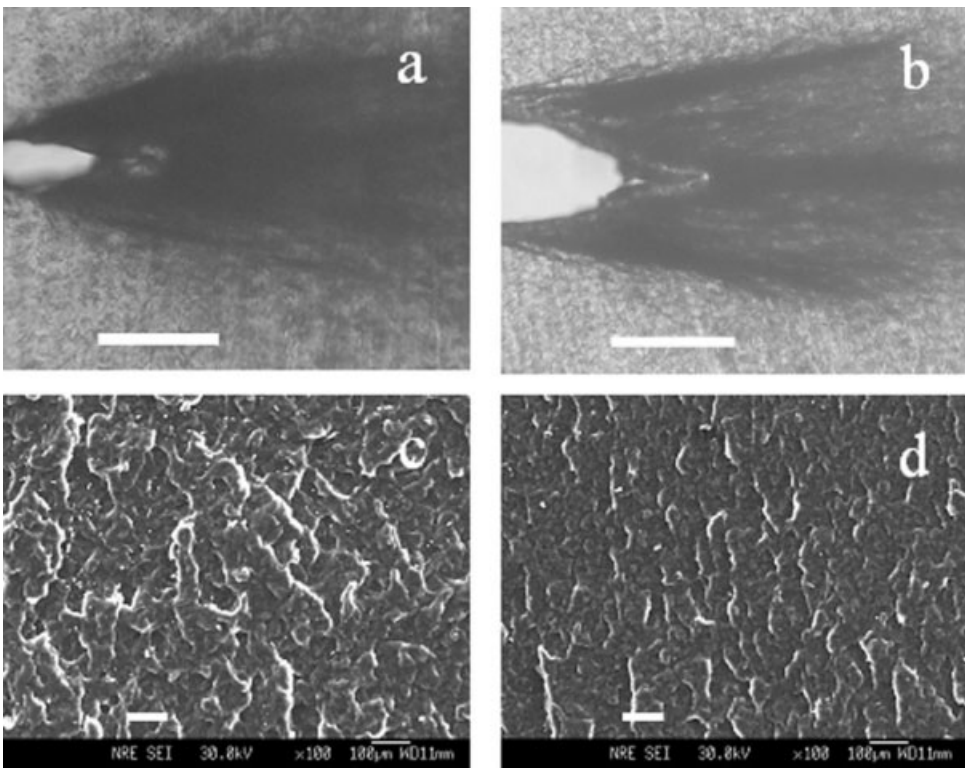

Figure 8 TOM (a, b) and SEM (c,d) micrographs revealing crack propagation (from left to right) in the γ-iPP (a, c) and α-iPP (b, d) sample, respectively. The scale bar is 100 μm.

amorphous phase on its growing front.[25] Significant network relaxation, mostly due to chain pullout from adhered crystals, can promote void propagation,[26] which is the exact situation for the α-iPP sample.

Failure and toughness

Two methods are adopted to characterize the toughness: one is notched Izod impact test with a loading speed of 3.5 m/s and the other is quasi-static EWF measurements at a tensile speed of 2 mm/min. The notched impact strength is 10.6 ± 1.4 and 7.8 ± 1.2 kJ/m^2 for the γ-iPP and α-iPP sample, respectively. Similar results are also obtained from EWF tests shown in Figure 7. The deduced specific EWF w_e, an intrinsic parameter evaluating the toughness of a ductile material, is 23.2 and 15.9 kJ/m^2 for γ-iPP and α-iPP sample, respectively. Note that the different value of toughness obtained by above-mentioned methods may result from different loading speed, sample geometry, and stress state (which is plane strain for Izod impact test and plane stress for EWF test, respectively). To further understand the fracture mechanism, damage zones ahead of notches in the γ-iPP and α-iPP sample, respectively, are examined on the DENT samples with quasi-static loading, as shown by the TOM photographs in Figure 8. Apparently, multiple and high-density crazes ahead of crack tip occur in the γ-iPP sample with higher toughness. Moreover, more significant crack blunting is observed in the γ-iPP sample, an indicator of higher crack propagation resistance. Similarly, rougher fracture surface in the initiation zone ahead of notches is observed in the γ-iPP sample while subjected to the Izod impact test with high-speed loading, as shown by the SEM photographs in Figure 8. Combination with the structural evolution under tension, therefore, it can be deduced that superior toughness in the γ-iPP sample should be directly originated from less network relaxation due to its higher fraction of tie chains interconnecting adjacent lamellae. Less network relaxation can sustain external force more effectively until the rupture of molecular chains and thus absorb more energy.[27] On the other hand, suppressed transverse void propagation in the γ-iPP sample should be responsible for its higher toughness in an indirect way because microporosity from cavitation can reduce the solid fraction of load-bearing materials at the crack tip. It is desired to note that the structural evolution at a crack tip is more severe than that encountered during stretching due to stress concentration and thus a notched sample usually fails in premature. However, it is difficult to real-time monitor the structural evolution during fracture tests even at quasi-static loading due to small damage zone ahead of a crack tip.[28,29] Therefore, complete understanding of the

relationship between structure and fracture toughness in γ-iPP sample still remains a challenge, which is the subject of our further work.

CONCLUSION

The dominant role of network relaxation in the void propagation and fracture of isotactic polypropylene has been explored. Less network relaxation, related to its peculiar crystalline and amorphous phases, is directly responsible for slower void propagation and higher toughness in the γ-iPP sample. The suppressed void propagation, in turn, also contributes to the increased toughness in the γ-iPP sample due to reduced void coalescence at a crack tip.

References

1. Koike, Y.; Cakmak, M. Polymer 2003, 44, 4249.
2. Schrauwen, B. A. G.; Janssen, R. P. M.; Govaert, L. E.; Meijer, H. E. H. Macromolecules 2004, 37, 6069.
3. Ouederni, M.; Phillips, P. J. J Polym Sci Polym Phys 1995, 33, 1313.
4. Song, Y.; Nemoto, N. Polymer 2005, 46, 6522.
5. Haward, R. N. Macromolecules 1993, 26, 5860.
6. Pawlak, A.; Galeski, A. Macromolecules 2005, 38, 9688.
7. Duffo, P.; Monasse, B.; Haudin, J. M.; G'sell, C.; Dahoun, A. J. Mater Sci 1995, 30, 701.
8. Li, J. X.; Cheung, W. L.; Chan, C. M. Polymer 1999, 40, 2089.
9. Pawlak, A.; Galeski, A. Macromolecules 2008, 41, 2839.
10. De Rosa, C.; Auriemma, F.; De Ballesteros, O.; Resconi, L.; Camurati, I. Macromolecules 2007, 40, 6600.
11. Hosier, I. L.; Alamo, R. G.; Esteso, P.; Isasi, J. R.; Mandelkern, L. Macromolecules 2003, 36, 5623.
12. Ferro, D. R.; Brückner, S.; Meille, S. V.; Ragazzi, M. Macromolecules 1992, 25, 5231.
13. Thomann, R.; Semke, H.; Maier, R. D.; Thomann, Y.; Scherble, J.; Mülhaupt, R.; Kressler, J. Polymer 2001, 42, 4597.
14. Lezak, E.; Bartczak, Z.; Galeski, A. Macromolecules 2006, 39, 4811.
15. Na, B.; Lv, R. J. Appl Polym Sci 2007, 105, 3274.
16. Lach, R.; Schneider, K.; Weidisch, R.; Janke, A.; Knoll, K. Eur Polym J 2005, 41, 383.
17. Thomann, R.; Wang, C.; Kressler, J.; Mülhaupt, R. Macromolecules 1996, 29, 8425.
18. Hiss, R.; Hobeika, S.; Lynn, C.; Strobl, G. Macromolecules 1999, 32, 4390.
19. Na, B.; Lv, R.; Xu, W.; Yu, P.; Wang, K.; Fu, Q. J. Phys Chem B 2007, 111, 13206.
20. De Rosa, C.; Auriemma, F.; De Ballesteros, O. R.; De Luca, D.; Resconi, L. Macromolecules 2008, 41, 2172.
21. Addiego, F.; Dahoun, A.; G'sell, C.; Hiver, J. Polymer 2006, 47, 4387.
22. Pawlak, A. Polymer 2007, 48, 1397.
23. Ijichi, Y.; Kojima, T.; Suzuki, Y.; Nishio, T.; Kakugo, M.; Amemiya, Y. Macromolecules 1993, 26, 829.
24. Yamashita, T.; Nabeshima, Y. Polymer 2000, 41, 6067.
25. Brady, J. M.; Thomas, E. L. J. Mater Sci 1989, 24, 3311.
26. Thomas, E. L., Ed. Structure and Properties of Polymers; VCH: Weinheim, 1993.
27. Brown, E. N.; Dattelbaum, D. M. Polymer 2005, 46, 3056.
28. Adriaensens, P.; Storme, L.; Carleer, R.; Vanderzande, D.; Gelan, J.; Litvinov, V. M.; Marissen, R. Macromolecules 2000, 33, 4836.
29. Maier, G. A.; Wallner, G.; Lang, R. W.; Fratzl, P. Macromolecules 2005, 38, 6099.